

Submitted to *Energy and Environmental Science* as a communication

## Supplemental

### Characterizations details.

Scanning Electron Microscopy (SEM) observations were performed with a Hitachi TM-1000 apparatus at 15 kV. The specimens were sputtered with Au/Pd prior to examination. Intrusion/extrusion mercury measurements were performed using a Micromeritics Autopore IV apparatus in order to assess the scaffolds' macrocellular cells characteristics. Small Angle X-ray Scattering (SAXS) experiments were carried on a 18 kW rotating anode X-ray source (Rigaku-200) with use of Ge (111) crystal as monochromator. The scattered radiation was collected on a two dimensional detector (Imaging Plate system from Mar Research, Hamburg). The sample- detector distance was 500 mm. Surface areas and pore characteristics at the micro- and mesoscale were obtained through nitrogen adsorption-desorption experiments using a Micromeritics ASAP 2010.  $^{29}\text{Si}$  Nuclear Magnetic Resonance (NMR) spectra were recorded on a Bruker Avance III 300 spectrometer (7 T) operating at 59.6 MHz. Samples were spun at 5 kHz using 7 mm  $\text{ZrO}_2$  rotors. The  $^{29}\text{Si}$  MAS NMR spectra were performed with a  $90^\circ$  pulse of 5  $\mu\text{s}$  and a recycle delay of 150 s. The spectra were deconvoluted with the DMFIT program [1].

### Supplementary results.

Biohybrid monolithic columns have been thoroughly characterized after use in continuous flow catalysis. For doing so, silica-based foams has been washed with distilled water and freeze-dried 24 hours, in order to keep as much as possible the structure of the hybrid framework. These macroporous materials have been examined by Scanning Electron Microscopy (SEM, Figure S1). Micrographs clearly reveal for both monolithic columns, the typical interconnected macroporous network of Si(HIPE)s materials, constituted of an aggregated hollow spheres-like macrostructure (hollow spheres are usually named *voids* or *cells*) [2]. This feature is mainly due to a privileged mineralization at the oil/water interface of

Submitted to *Energy and Environmental Science* as a communication

the soft template concentrated emulsion. Moreover, a high interconnectivity between *void spaces* is highlighted by internal junctions (see green solid arrow on Figure S1b), connecting two directly adjacent *cells*, and external junctions (see red dotted arrow on Figure S1b), induced by statistical aggregation of oil droplets during emulsification process.

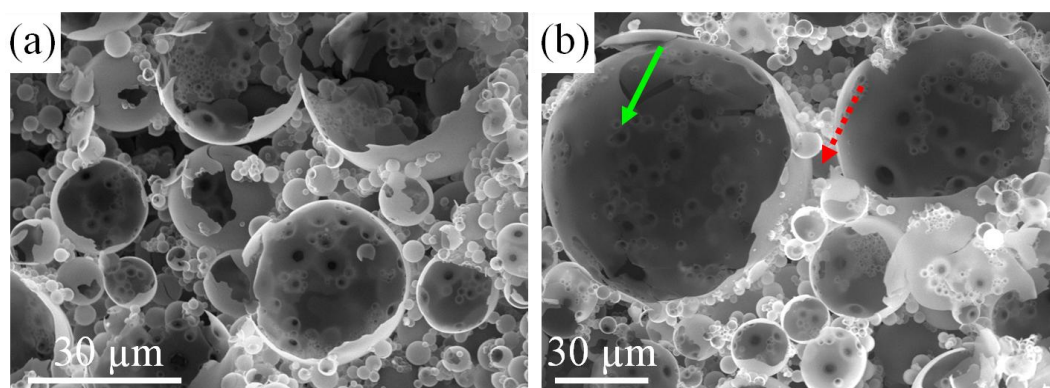


**Figure S1.** Scanning electron micrographs (SEM) of the biohybrid macroporous columns after continuous flow catalysis, washing and freeze-drying. (a) *Col*[C-CR-lipase]@gGlymo-Si(HIPE) and (b) *Col*[C-TL-lipase]@gGlymo-Si(HIPE). The green solid arrow indicates an internal cell junction, whereas the red dotted arrow corresponds to an external cell junction.

High interconnectivity between voids is also emphasized by mercury intrusion porosimetry data (Figure S2). At this stage, it is necessary to remind that mercury porosimetry provides only informations about the junctions, also named windows, that connect adjacent void spaces, and not on the cellular void spaces themselves. Pores size distribution for both monolithic columns exhibit a main windows diameter centered on 10  $\mu\text{m}$ , probably related to external junctions, together with a less-defined shoulder, between 100 nm and 2  $\mu\text{m}$ , feature that can be associated with narrow internal junctions (see arrows on Figure S2).

Submitted to *Energy and Environmental Science* as a communication

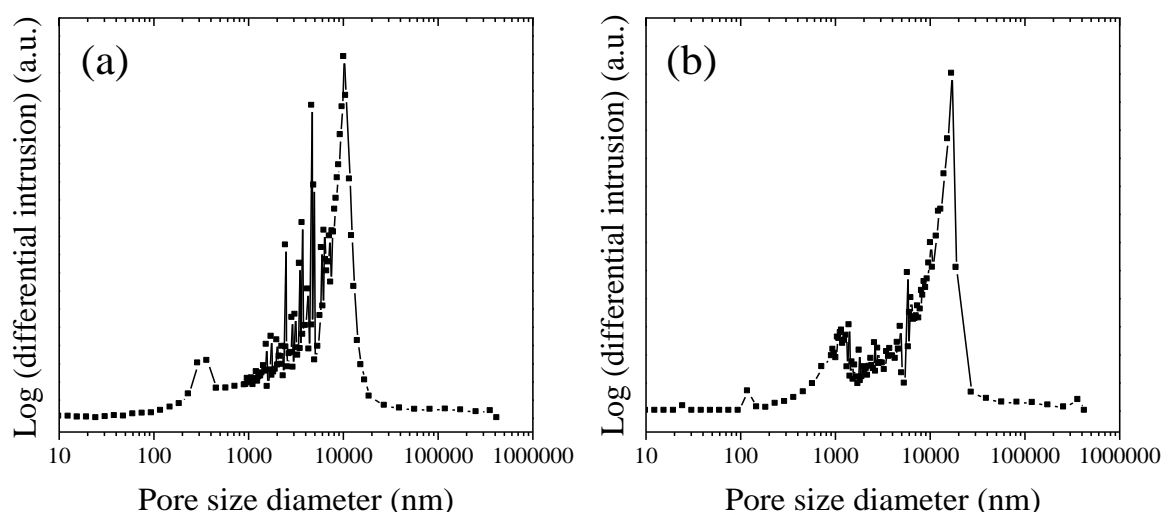


**Figure S2.** Pore size distributions of the biohybrid macroporous columns after continuous flow catalysis, washing and freeze-drying, determined by mercury intrusion porosimetry. (a) *Col*[C-*CR*-lipase]@*gGlymo*-Si(HIPE) and (b) *Col*[C-*TL*-lipase]@*gGlymo*-Si(HIPE).

In conjunction with a high interconnectivity between void spaces, these biohybrid monolithic columns exhibit elevated macroporosities, close to 95 %, and intrusion volumes, up to  $20.1 \text{ cm}^{-3} \cdot \text{g}^{-1}$ , as revealed by mercury porosimetry data (Table S1). A higher skeletal density can be noticed for the *Col*[C-*TL*-lipase]@*gGlymo*-Si(HIPE). This feature will be discussed later.

**Table S1.** Mercury intrusion porosimetry data of the biohybrid macroporous columns after continuous flow catalysis, washing and freeze-drying.

Biohybrid foams	Porosity (%)	Intrusion volume ( $\text{cm}^{-3} \cdot \text{g}^{-1}$ )	Skeletal density ( $\text{g} \cdot \text{cm}^{-3}$ )
<i>Col</i> [C- <i>CR</i> -lipase]@ <i>gGlymo</i> -Si(HIPE)	95	20.0	1.0
<i>Col</i> [C- <i>TL</i> -lipase]@ <i>gGlymo</i> -Si(HIPE)	94	13.0	1.2

Beyond macroporosity, these foams exhibit some degree of mesoporosity, induced by supramolecular self-assembly of the cationic surfactants used to stabilize oil-water interfaces of the native concentrated emulsion. Indeed, small-angle X-ray scattering profiles (SAXS,

Submitted to *Energy and Environmental Science* as a communication

Figure S3) of these materials constantly depict a broad peak centered at a wave vector,  $q$ , of  $0.144 \text{ \AA}^{-1}$ . This feature clearly discloses a vermicular mesostructure, associated with an unit cell parameter around 4.4 nm, in agreement with previous results obtained for Si(HIPE)s without thermal treatment [2].

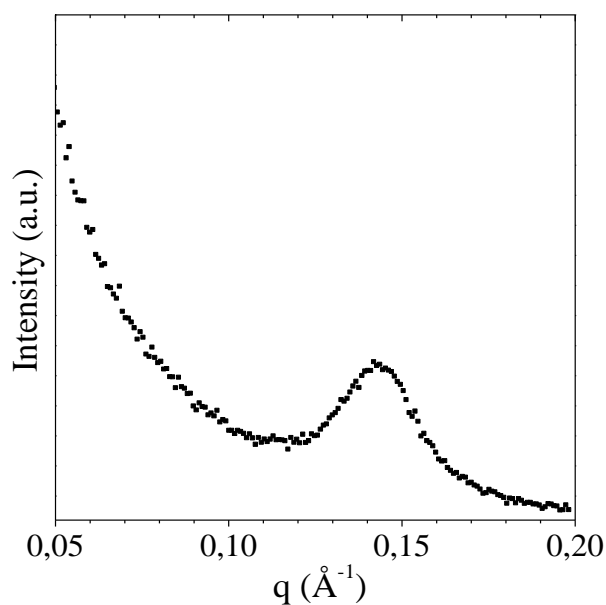


**Figure S3.** Small-angle X-ray scattering profile of a biohybrid macroporous column after continuous flow catalysis, washing and freeze-drying.

The presence of mesopores is also confirmed by nitrogen sorption experiments (Figure S4). Concerning the *Col*[C-CR-lipase]@*g*Glymo-Si(HIPE) sample, a mixed type II/ type IV isotherm can be noticed, exhibiting a hysteresis of the desorption curve compared with the adsorption one (Figure S4a). This hysteresis clearly highlights a capillary condensation phenomenon, induced by the presence of mesopores within the hybrid silica-based framework. Moreover, a fast rise of the nitrogen adsorption at the very low relative pressures (up to 0,04) involves a microporous component, while the progressive increase of the  $N_2$  amount adsorbed above relative pressure of 0.2 and up to 1.0, strongly suggests a multimolecular adsorption, relative to macropores (Figure S4a). On the other hand, the nitrogen sorption curve noticed for the *Col*[C-TL-lipase]@*g*Glymo-Si(HIPE) sample depicts a

Submitted to *Energy and Environmental Science* as a communication

type II isotherm, strongly suggestive of an essentially macroporous material (Figure S4c). The lack of a fast N<sub>2</sub> sorption rise at the very low relative pressures implies an absence or a minor accessibility of micropores. The pore size distributions, obtained by density functional theory for both hybrid foams (Figure S4b-d), show constantly a broad peak centered at 3-4 nm, in agreement with SAXS data (Figure S4). Nevertheless, a less marked hysteresis is discernible for the *Col*[C-*TL*-lipase]@*g*Glymo-Si(HIPE), suggesting a reduced accessibility to the mesoporous component.

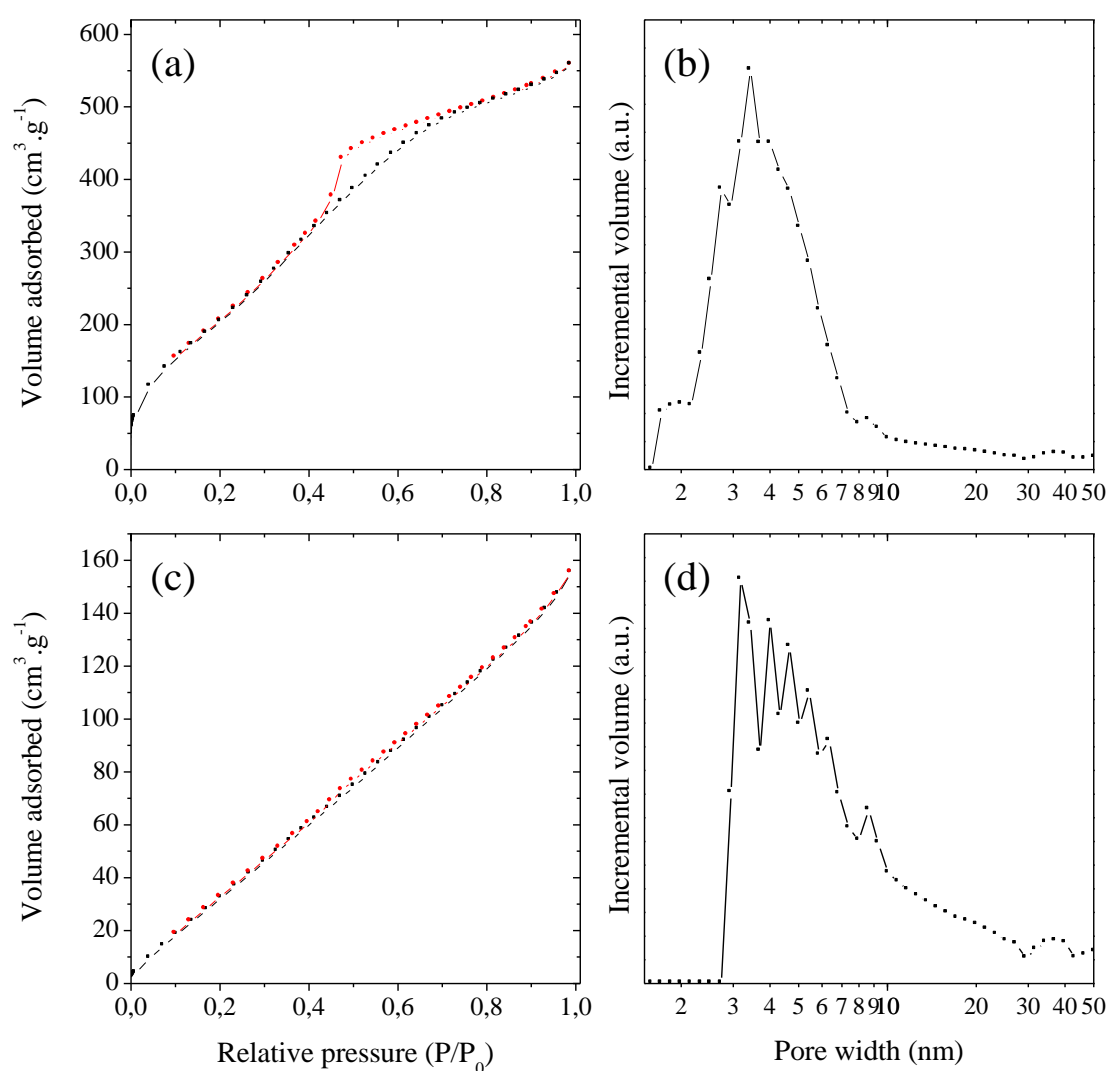


**Figure S4.** Nitrogen sorption isotherms for (a) *Col*[C-*CR*-lipase]@*g*Glymo-Si(HIPE) and (c) *Col*[C-*TL*-lipase]@*g*Glymo-Si(HIPE). Pore size distributions obtained by Density Functional Theory (DFT) for (b) *Col*[C-*CR*-lipase]@*g*Glymo-Si(HIPE) and (d) *Col*[C-*TL*-lipase]@*g*Glymo-Si(HIPE).

Submitted to *Energy and Environmental Science* as a communication

These features can be explained by a larger amount of biomolecules within the *Col*[C-*TL*-lipase]@*g*Glymo-Si(HIPE) hybrid framework, inducing a partial obstruction of nitrogen molecules towards the smaller pores (typically, micro- and mesopores). This characteristic, confirmed by both Brunauer, Emmett, Teller (BET) and Barret, Joyner, Halenda (BJH) data (Table S2), will be discussed by comparing stoichiometries and enzymatic loadings of each column.

**Table S2.** Nitrogen sorption data for the biohybrid macroporous columns after continuous flow catalysis, washing and freeze-drying.

Biohybrid foams	BET surface area (m <sup>2</sup> .g <sup>-1</sup> ) <sup>a</sup>	Mesoporous surface area (m <sup>2</sup> .g <sup>-1</sup> ) <sup>b</sup>	Total porous volume (cm <sup>3</sup> .g <sup>-1</sup> ) <sup>c</sup>	Mesoporous volume (cm <sup>3</sup> .g <sup>-1</sup> ) <sup>b</sup>
<i>Col</i> [C- <i>CR</i> -lipase]@ <i>g</i> Glymo-Si(HIPE)	962	541	0.86	0.61
<i>Col</i> [C- <i>TL</i> -lipase]@ <i>g</i> Glymo-Si(HIPE)	210	143	0.24	0.21

<sup>a</sup> calculated using the BET model, <sup>b</sup> calculated using the BJH model, <sup>c</sup> calculated using the single point model

To quantify the degree of grafting and condensation of organosilane derivatives (epoxy groups) anchored within the silica-based frameworks, a study by <sup>29</sup>Si nuclear magnetic resonance (NMR) at the magic angle spinning (MAS), was conducted (Figure S5 and Table S3). <sup>29</sup>Si sites are labeled with the conventional T<sub>n</sub> and Q<sub>n</sub> notations. T refers to functional (R)SiO<sub>n</sub>(OH)<sub>3-n</sub> units, induced by organosilane precursors grafting, and Q to SiO<sub>n</sub>(OH)<sub>4-n</sub> units, associated with native silica-based scaffold (n being the number of bridging oxygen atoms, generated by the condensation process, surrounding the silicon). Chemical shifts were determined relative to TMS (tetramethylsilane). Due to the presence of both the T<sub>n</sub> and Q<sub>n</sub> signals, the efficient grafting of the organosilane derivative is confirmed for both monolithic porous microreactors (Figure S5).

Submitted to *Energy and Environmental Science* as a communication

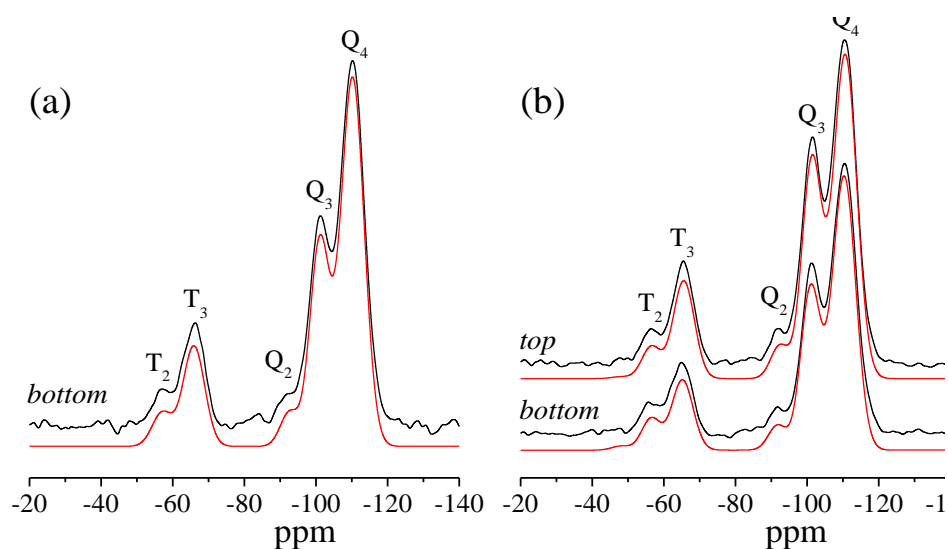


**Figure S5.** <sup>29</sup>Si nuclear magnetic resonance spectra obtained at the magic angle spinning for (a) *Col*[C-CR-lipase]@*g*Glymo-Si(HIPE) and (b) *Col*[C-TL-lipase]@*g*Glymo-Si(HIPE). NMR MAS experiments have been performed at the lower part (*bottom*), together with the upper part (*top*) of the *Col*[C-TL-lipase]@*g*Glymo-Si(HIPE) column.

After a Lorentzian/Gaussian deconvolution of the NMR spectra, atomic compositions in T<sub>n</sub> and Q<sub>n</sub> species can be determined (Table S3). Thus, concerning both grafting (T<sub>n</sub> / (T<sub>n</sub>+Q<sub>n</sub>)) and condensation (T<sub>3</sub> / T<sub>2</sub>) degrees, no difference can be noticed between the two hybrid columns, revealing a good reproducibility of the continuous flow functionalization process. Moreover, no grafting gradient can be observed between the lower and the upper parts of the as-synthesized biohybrid *Col*[C-TL-lipase]@*g*Glymo-Si(HIPE), suggesting an homogeneous functionalization within the porous scaffold.

Submitted to *Energy and Environmental Science* as a communication

**Table S3.** Molar percentages of Q<sub>n</sub> and T<sub>n</sub> units and molar ratio T<sub>3</sub> / T<sub>2</sub> (condensation degree) calculated from the integration of NMR peaks after a Lorentzian/Gaussian deconvolution. NMR MAS experiments have been performed at the lower part (*bottom*), together with the upper part (*up*) of the Col[C-TL-lipase]@gGlymo-Si(HIPE) column.

Biohybrid foams		RMN MAS <sup>29</sup> Si		
		% Q <sub>n</sub>	% T <sub>n</sub>	T <sub>3</sub> / T <sub>2</sub>
Col[C-CR-lipase] @gGlymo-Si(HIPE)	<i>bottom</i>	82.2	17.8	3.2
Col[C-TL-lipase] @gGlymo-Si(HIPE)	<i>bottom</i>	82.0	18.0	2.5
	<i>up</i>	80.5	19.5	3.2

Beyond organosilane precursors grafting, the enzymatic loadings were determined by the Bradford [3] assay using bovine serum albumin as a standard, checking the protein content of both impregnation and washing solutions. At this stage, it can be noticed that a larger amount of lipases has been immobilized within the Col[C-TL-lipase]@gGlymo-Si(HIPE) foam. This feature is mainly explained by the two-step procedure, involving an intermediate activation of the biohybrid macroporous monolith with a 5% w./v. glutaraldehyde aqueous solution. Indeed, the formation of Cross-Linked Enzyme Aggregates (CLEAs) [4], covalently bonded *via* glutaraldehyde's bridges, can be strongly suggested. The overall biohybrid column stoichiometries can be found within table S4.

**Table S4.** Lipase loadings and stoichiometries of the biohybrid columns determined by both <sup>29</sup>Si nuclear magnetic resonance and Bradford assay.

Immobilized lipases	Stoichiometries <sup>c</sup>	
	Weight (mg)	
<i>Candida rugosa</i>	9.4 <sup>a</sup> (57 %) <sup>b</sup>	Col[C-CR-lipase] <sub>5.4.10<sup>-6</sup></sub> @SiO <sub>1.82</sub> (C <sub>6</sub> O <sub>2</sub> H <sub>11</sub> ) <sub>0.18</sub>
<i>Thermomyces lanuginosus</i>	158 <sup>a</sup> (81 %) <sup>b</sup>	Col[C-TL-lipase] <sub>1.7.10<sup>-4</sup></sub> @SiO <sub>1.82</sub> (C <sub>6</sub> O <sub>2</sub> H <sub>11</sub> ) <sub>0.18</sub>

<sup>a</sup>Amounts of enzymes immobilized determined by Bradford assay. <sup>b</sup>Percentages of enzymes immobilized related to the initial lipase weight used in the solution of impregnation.

We can notice that the enzyme loading is around one hundred times higher for the column Col[C-TL-lipase]@gGlymo-Si(HIPE) than the Col[C-CR-lipase]@gGlymo-Si(HIPE).

Submitted to *Energy and Environmental Science* as a communication

This feature has two consequences. First the higher enzyme loading will avoid nitrogen access to the mesoscopic void spaces when performing  $N_2$  adsorption-desorption measurement. As a direct consequence, the specific surface area should be smaller for the *Col*[C-CR-lipase]@*g*Glymo-Si(HIPE), as it is the case considering both figure S4 and table S2. Also, considering the high molecular weight of the protein in use, a loading higher with a factor 100 for the *Col*[C-TL-lipase]@*g*Glymo-Si(HIPE), will undoubtedly increase the foams skeletal density as it is observed above considering table S1, where mercury porosimetry results are summarized. Considering these hybrid foams, the effects of the embedded [5] or grafted [6] organic content over the final mesoporosity and skeletal density are well known and reported.

#### Examples of HPLC chromatograms.

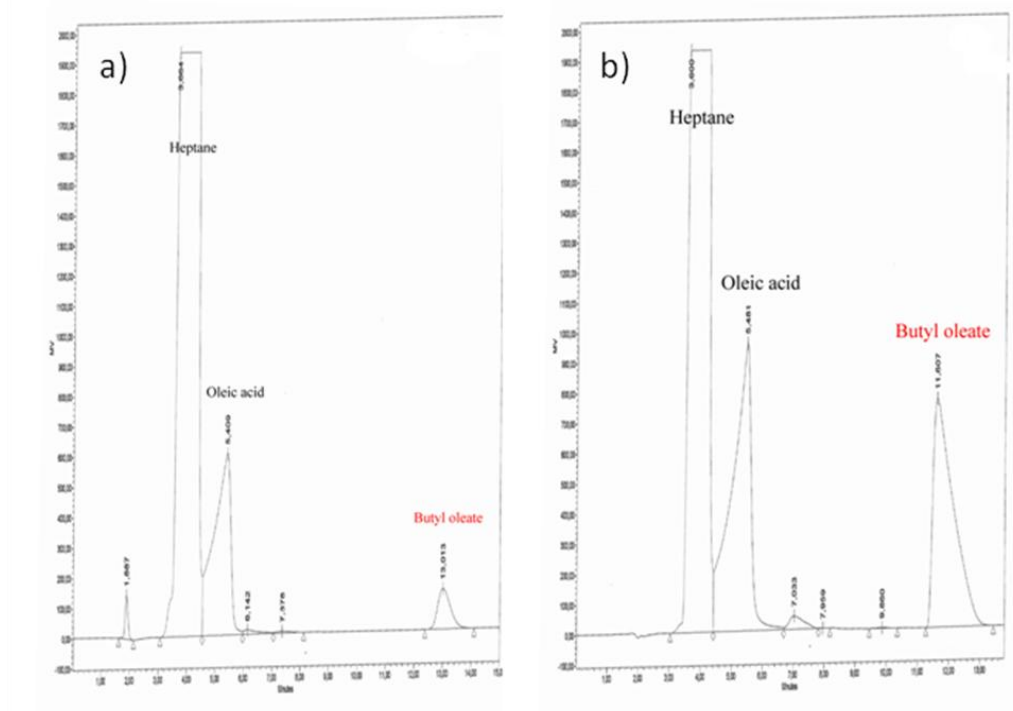


**Figure S6.** HPLC chromatograms a) after 6 days of esterification, b) after after 40 days of esterification.

Submitted to *Energy and Environmental Science* as a communication

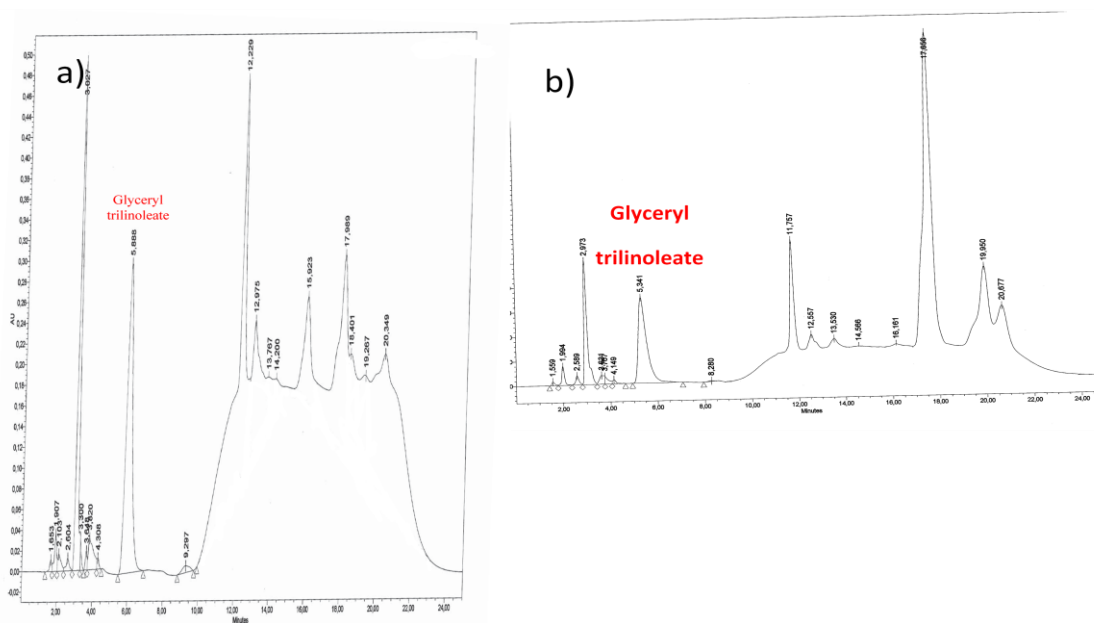


**Figure S7.** HPLC chromatograms a) after 10 days of transesterification, b) after after 60 days of transesterification.

## References

- [1] (a) R.K. Harris, M.L. Robbins, *Polymer* **1978**, *19*, 1123. (b) F. Babonneau, *New J. Chem.* **1994**, *18*, 1065. (c) Y. Chevalier, A.-C. Grillet, M.-I. Rahmi, C. Lière, M. Masure, P. Hémerly, F. Babonneau, *Mater. Sci. Engin. C* **2002**, *21*, 143.
- [2] F. Carn, A. Colin, M.-F. Achard, M. Birot, H. Deleuze, R. Backov, *J. Mat. Chem.* **2004**, *14*, 1370.
- [3] M.M. Bradford, *Anal Biochem.* **1976**, *72*, 248.
- [4] B.C. Kim, S. Nair, J. Kim, J.H. Kwak, J.W. Grate, S.H. Kim, M.B. Gu, *Nanotechnology* **2005**, *16*, S382.
- [5] S. Ungureanu, M. Birot, L. Guillaume, H. Deleuze, O. Babot, B. Julian-Lopez, M.-F. Achard, M. I. Popa, C. Sanchez, R. Backov, *Chem. Mater.* **2007**, *19*, 5786.
- [6] S. Ungureanu, H. Deleuze, M. I. Popa, C. Sanchez, R. Backov, *Chem. Mater.* **2008**, *20*, 6494.